Check for updates

Production of solar abundances for nuclei beyond Sr: The *s*- and *r*-process perspectives

Maurizio M. Busso[1,2]*, Karl-Ludwig Kratz[3,4], Sara Palmerini[1,2,5], Waheed Akram[6] and Vincenzo Antonuccio-Delogu[7]

[1]Department of Physics and Geology, University of Perugia, Perugia, Italy, [2]INFN, Section of Perugia, Perugia, Italy, [3]Department of Chemistry, Pharmacy and Geosciences, University of Mainz, Mainz, Germany, [4]Max-Planck-Institut für Chemie, Hahn-Meitner-Weg 1, Mainz, Germany, [5]INAF, Astronomical Observatory of Rome, Rome, Italy, [6]Department of Earth Sciences, University of Oxford, Oxford, United Kingdom, [7]INAF, Astrophysical Observatory of Catania, Catania, Italy

We present the status of nucleosynthesis beyond Sr, using up-to-date nuclear inputs for both the slow (*s*-process) and rapid (*r*-process) scenarios of neutron captures. It is now widely accepted that at least a crucial part of the *r*-process distribution is linked to neutron star merger (*NSM*) events. However, so far, we have found only a single direct observation of such a link, the kilonova GW170817. Its fast evolution could not provide strict constraints on the nucleosynthesis details, and in any case, there remain uncertainties in the local *r*-process abundance patterns, which are independent of the specific astrophysical site, being rooted in nuclear physics. We, therefore, estimate the contributions from the *r*-process to solar system (*S.S.*) abundances by adopting the largely site-independent *waiting-point* concept through a superposition of neutron density components normalized to the *r*-abundance peaks. Nuclear physics inputs for such calculations are understood only for the trans-Fe nuclei; hence, we restrict our computations to the Sr−Pr region. We then estimate the *s*-process contributions to that atomic mass range from recent models of asymptotic giant branch stars, for which uncertainties are known to be dominated by nuclear effects. The outcomes from the two independent approaches are then critically analyzed. Despite the remaining problems from both sides, they reveal a surprisingly good agreement, with limited local discrepancies. These few cases are then discussed. New measurements in ionized plasmas are suggested as a source of improvement, with emphasis on *β*-decays from unstable Cs isotopes. For heavier nuclei, difficulties grow as *r*-process progenitors lie far off experimental reach and poorly known branchings affect *s*-processing. This primarily concerns nuclei that are significantly long-lived in the laboratory and have uncertain decay rates in stars, e.g., [176]Lu and [187]Re. New measurements are urgently needed for them, too.

KEYWORDS

nuclear astrophysics, weak interactions, nucleosynthesis, s-processes, r-processes, stars

1 Introduction

Based on the first detailed geochemical abundance determinations of Suess and Urey (1956), the neutron shell structure investigations of Coryell (1956; 1961), and the discovery of radioactive Tc in the photospheres of evolved red giants (Merrill, 1952), the seminal works of Burbidge et al. (1957) (B^2FH) and Cameron (1957) laid down the fundamental astrophysical conditions for the production of heavy elements. This included, in particular, isotopes beyond Fe, which were found in those works to be synthesized by neutron-capture processes, either slow (the *slow* or *s*-process) or fast (the *rapid* or *r*-process). Here, the terms *slow* and *rapid* consider whether neutron captures proceed at rates slower or faster than those of typical β-decays occurring along the respective nucleosynthesis path.

The *slow* neutron captures (in particular, their *main* component, including isotopes across and beyond the neutron magic number $N = 50$ up to $N = 126$) were attributed to the final evolutionary stages of red giants (called *asymptotic giant branch* or AGB stars). This was possible owing to the demonstration by Ulrich (1973) that their repeated ignition of He burning in a thin, unstable shell offered a natural way to produce the exponentially decreasing distribution of neutron exposures, previously invoked by Seeger et al. (1965).

Afterward, several attempts were made in the 70s, adopting intermediate-mass stars (see Iben and Truran, 1978) (IMS) models ($4 \leq M/M_\odot \leq 8$) as s-process sites. There, the ^{22}Ne(α,n)^{25}Mg source can be easily activated. However, the excessive neutron densities ($n_n \geq 10^{11} cm^{-3}$) it generated at the local temperatures ($T \simeq 3.5 10^8 cm^{-3}$) were shown to be incompatible with observations (Busso et al., 1988) so that lower-mass ($M/M_\odot \leq 3$) AGB stars were finally considered (Iben and Renzini, 1982; Gallino et al., 1988). This implied assuming that the alternative ^{13}C(α,n)^{16}O neutron source (requiring lower temperatures and producing lower n_n values, around $10^7 cm^{-3}$) could be activated, as a consequence of some partial diffusion of protons from the envelope, sufficient to produce ^{13}C in the He-rich layers when the H-burning shell reignites.

This ^{13}C(α,n)^{16}O neutron source had been suggested to be at play many years before by Cameron (1957), but even now, the elusive mixing mechanisms necessary to its activation remain a subject of active research. Many attempts were dedicated along the past three decades to this goal, often on parametric grounds (Käppeler et al., 2011; Bisterzo et al., 2012), simulating various deep mixing events (Bisterzo et al., 2014, 2015; Cristallo et al., 2015; Battino et al., 2019). Partial accounts of these efforts can be found in Busso et al. (1999); Busso et al. (2007); Karakas and Lattanzio (2014); and Busso et al. (2021).

In particular, in the present study, we shall concentrate on results obtained in a recent series of models, where the formation of the mentioned neutron source was attributed to the buoyancy

of magnetic flux tubes maintained by a dynamo process (Nucci and Busso, 2014).

For what concerns fast neutron captures, the same studies by Burbidge et al. (1957) and Cameron (1957) outlined a reasonable scenario for the first time. In these early studies, a steady-state formation of isotopes by neutron addition and hold-ups for nuclei with shells at $N = 50$, 82, or 126 neutrons was already postulated. This is presently better known as the *r*-process *waiting-point concept*. Since then, *r*-process research works have been quite diverse in terms of suggested stellar scenarios (for representative historical reviews, see Seeger et al., 1965; Hillebrandt, 1978; Kratz, 1988; Cowan et al., 1991; Kratz et al., 1993).

While for several decades the high-entropy (ν-driven) winds from core collapse supernovae type II (*ccSN-II*) were proposed as the favored r-process site (see Takahashi et al., 1994; Woosley et al., 1994; Freiburghaus et al., 1999a; Kratz et al., 2008; Farouqi et al., 2010; Kratz et al., 2014), attention was also given to complementary scenarios, in particular to the decompressed ejecta of neutron star mergers (*NSM*), which were discussed in important articles since the early epochs (Lattimer et al., 1977; Freiburghaus et al., 1999b; Rosswog et al., 1999).

However, still in the early 1990s, none of the suggested r-process scenarios could yield satisfactory results to fit the solar system (*S.S.*) r-process abundances. Hence, the Mainz −Basel −Los Alamos collaboration started to use improved site-independent calculations (Kratz et al., 1993). Although not (yet) pointed out explicitly in that work, these attempts also implied the possible existence of several r-process sites with different abundance patterns. Therefore, the S.S. abundances generated by fast neutron captures had to be explained by a superposition of r-process components, with varying neutron densities n_n (with $n_n \geq 10^{20}$ cm^{-3}), and occurring on time scales between 1 and 2 s.

First experimental information on anomalous local abundance yields of an unknown nucleosynthesis origin and corresponding attempts to determine their astrophysical conditions were from cosmochemical isotopic measurements in meteoritic *CAI*, together with presolar SiC − X grains and nanodiamonds (see Wasserburg et al., 1977; Niederer et al., 1980; Kratz et al., 2001; Pellin et al., 2006; Farouqi et al., 2009). In addition, *elemental* abundances were determined in metal-poor halo stars (for early articles, see Sneden et al., 1996, 2003; Hill et al., 2002; Honda et al., 2007; Mashonkina et al., 2007).

Initially, the suggested sites were based on a rather indirect way on nucleosynthesis modeling. Early research works suggested that light and intermediate trans-Fe elements could be synthesized due to a "weak r-process" component, while the heavier elements up to the $A = 195$ peak and the actinides could be synthesized in a "main r-process" variant. Recently, observations of gravitational waves from an *NSM* event (GW170817 see Abbott et al., 2017), together with the subsequent electromagnetic emission from a kilonova (see

Evans et al., 2017), showed the first direct evidence of the ongoing *r*-process nucleosynthesis (Rosswog et al., 2018). Based on the emission of the red wavelength lanthanide fraction, Ji et al. (2019) suggested however that this *NSM* event did not actually produce a typical S.S. *r* pattern: further observations of similar objects are needed to draw firmer conclusions.

In order to accumulate sufficient information on the various *r*-process contributions from heterogeneous sources, today, systematic and accurate observational constraints from many low-metallicity stars exist (see the *HERES* survey (Hamburg ESO R-process Enhanced Star) Mashonkina and Christlieb, 2014) and provide adequate databases for comparing model results.

In the present study, after recalling briefly the results of recent work on *n*-captures, the status of heavy-element production is studied by verifying the compatibility of the scenarios for *s*- and *r*-process nucleosynthesis, through a comparison of their respective predictions for the S.S. composition. With this goal in mind, the mentioned research on the classical *waiting-point* approach (Kratz et al., 2007) turned out to be of special relevance, as it can exclude uncertainties related to the modeling of specific sites.

Reasonably good nuclear inputs for this work are available only below $A \simeq 140$–142, so this is the mass range on which we focus. Predictions from fast neutron captures are then compared to those for *s*-processing in AGB stars of low mass (namely, for masses $M = 1.3, 1.5, 2.0,$ and $3.0\ M_\odot$, computed at metallicities from [Fe/H] = 0.1 down to [Fe/H] = − 0.8), after weighting on the classical Salpeter's initial mass function (IMF) (Salpeter, 1955) and on the star formation rate (SFR) from Maiorca et al. (2012). Thus, we infer some new hints, including suggestions for future measurements.

A short outline of the adopted *s*-process models and of their predictions is presented in Section 2, while in Section 3, we discuss the assumptions for the *waiting-point* scenario of *r*-processing. The good agreement found between these complementary, independent views and the residual problems emerging are then outlined in Section 4, where improvements expected from future *β*-decay rate measurements are also underlined. Preliminary conclusions are drawn in Section 5.
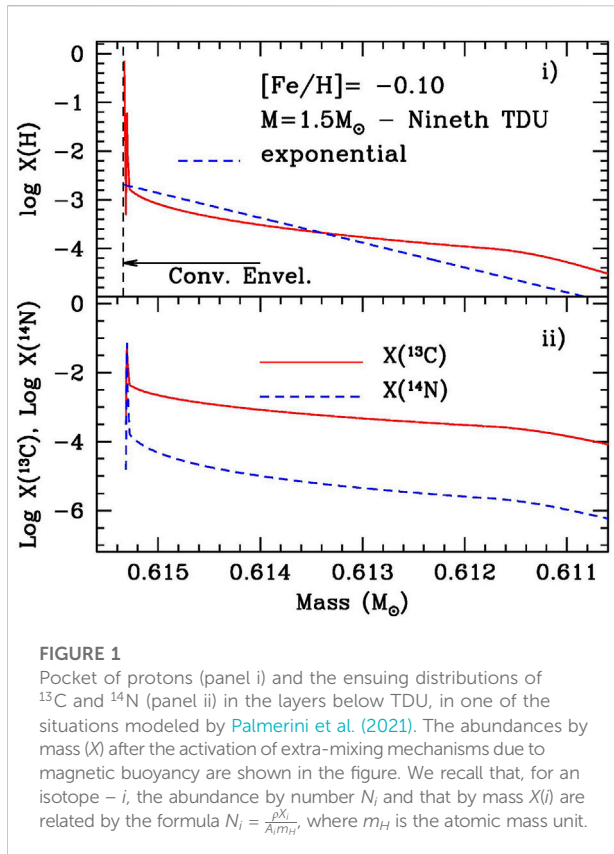
2 A model for slow neutron captures and its results

In recent studies, revisions on the status of slow neutron captures, as occurring in evolved stars of low mass ($1.3 \lesssim M/M_\odot \lesssim 3$) during the *AGB* stages, were discussed. These works deal with the particular approach that considers the buoyancy of magnetic flux tubes in a stellar dynamo process as responsible for the deep mixing episodes mentioned in Section 1 (see Nordhaus et al., 2008; Denissenkov et al., 2009). This idea led to analytical models of the underlying physical mechanisms in terms of 3D solutions for the magneto-hydrodynamic (MHD) equations involved

(Nucci and Busso, 2014), where the previously quoted recent upgrades were obtained with the help of full stellar models (Vescovi et al., 2020; Vescovi, 2021), subsequently integrated by post-process computations, derived with the aim of reproducing the relevant physical parameters without recomputing the energy generation (Busso et al., 2021). In those attempts, comparisons were presented between model predictions and some major available constraints to *s*-processing (from high-resolution spectroscopy of selected classes of evolved stars to the *S.S.* abundances as emerging from the chemical evolution of the Galaxy and to isotopic admixtures of heavy elements, as measured in presolar grains recovered in pristine meteorites). In that first analysis, the input data for cross-sections of stable isotopes were mainly obtained from the Kadonis 0.3 repository (Dillmann et al., 2006), partly integrated with more recent measurements. For radioactive nuclei, cross-sections were taken from Shibata et al. (2011) (*jend4.0*), while rates for $\beta^\pm$ decays and electron captures were from Takahashi and Yokoi (1987). The global accord obtained in that work between model predictions and S.S. abundances for *s*-only nuclei appeared to be fair, with a dispersion of model data roughly at the same level as measurement uncertainties (around $\sigma \simeq$ 15%). Also, general indications from other constraints suggested a reasonable agreement, although not much could be said on possible further improvements and on discrepancies for individual isotopes.

Recent research on nuclear cross-sections, on the other hand, pointed out that substantial work is still needed in that field, both through real new estimates and through reanalysis of existing datasets (e.g., by Monte Carlo techniques) (Reifarth et al., 2018). Partial results from this work have recently been used (Vescovi and Reifarth, 2021) to study the impact on nuclear upgrades in stellar models. So far, however, a global update of the Kadonis compilation is still waited for. For the aforementioned reasons, it is important that also from the point of view of stellar modeling, a search must be pursued for better constraints on nuclear parameters. Palmerini et al. (2021), in particular, adopted the compilation of cross-sections Kadonis 1.0 (Dillmann, 2014) and made a detailed comparison between stellar predictions from specific masses and metallicities and the record of isotopic anomalies measured in presolar SiC grains (Liu et al., 2015; Stephan et al., 2018), covering the atomic mass interval from Sr to Ba (again, A ≲ 140). The analysis was, in particular, useful to verify the rather detailed agreement that could be reached and, at the same time, to indicate the need for revisions of some weak interactions, e.g., suggesting new measurements for the *β*-decay rates of Cs isotopes in ionized environments (see also Mascali et al., 2020; Li et al., 2021; Taioli et al., 2021).

As mentioned, the upgrades by Busso et al. (2021) and Palmerini et al. (2021) were based on the idea that, during the so-called *third dredge-up* or *TDU* episodes (see Lugaro et al., 2012; Karakas and Lattanzio, 2014), MHD mechanisms maintained by dynamo cycles

FIGURE 1
Pocket of protons (panel i) and the ensuing distributions of
^{13}C and ^{14}N (panel ii) in the layers below TDU, in one of the
situations modeled by Palmerini et al. (2021). The abundances by
mass (X) after the activation of extra-mixing mechanisms due to
magnetic buoyancy are shown in the figure. We recall that, for an
isotope $-i$, the abundance by number N_i and that by mass $X(i)$ are
related by the formula $N_i = \frac{\rho X_i}{A_i m_H}$, where m_H is the atomic mass unit.

TABLE 1 Predictions of the fractional solar abundances from fast and
slow n-captures ($88 \leq A \leq 142$).

Z	A	Element	N(S.S.)	S.S. r – %	S.S. s – %	AGB s – %
38	88	Sr	19.2	10.2	89.8	89.2
39	89	Y	4.35	23.8	76.2	78.6
40	90	Zr	5.621	34.5	65.5	66.9
—	91	—	1.226	36.1	63.9	72.8
—	92	—	1.873	35.4	64.6	72.2
—	94	—	1.899	17.1	82.9	92.1
—	96	—	0.306	95.7	4.4	8.40
41	93	Nb	0.780	33.8	66.2	58.7
42	95	Mo	0.412	53.9	46.1	42.7
—	97	—	0.249	51.0	49.0	45.4
—	98	—	0.630	57.7	42.3	75.7
—	100	—	0.253	97.2	2.8	(< 1)
44	99	Ru	0.230	69.6	30.4	24.9
—	101	—	0.228	81.2	18.8	15.6
—	102	—	0.570	37.9	62.1	42.8
—	104	—	0.336	100	(< 1)	4
45	103	Rh	0.338	83.0	17.0	13.1
46	105	Pd	0.3079	83.4	16.6	14.0
—	106	—	0.377	73.9	26.1	50.7
—	108	—	0.365	47.8	52.2	63.23
—	110	—	0.162	100	(< 1)	5
47	107	Ag	0.258	79.1	20.9	14.8
—	109	—	0.239	82.6	17.4	24.8
48	111	Cd	0.202	81.1	18.9	24.2
—	112	—	0.381	44.2	52.8	51.5
—	113	—	0.193	65.4	34.6	35.6
—	114	—	0.454	36.1	63.9	64.5
—	116	—	0.119	92.1	7.9	18.3
49	115	—	0.171	63.1	36.9	36.9
50	117	Sn	0.276	47.3	52.7	50.6
—	118	—	0.870	63.1	36.9	76.2
—	119	—	0.308	49.6	50.4	41.2
—	120	—	1.171	19.8	80.2	85.1
—	122	—	0.166	61.5	38.5	40
—	124	—	0.208	100	(< 1)	(< 1)
51	121	Sb	0.205	67.3	32.7	40.0
—	123	—	0.154	96.0	4.0	(< 1)
52	125	Te	0.337	72.5	27.5	22.9
—	126	—	0.894	48.3	51.7	46.6
—	128	—	1.494	100	(< 1)	(< 1)
—	130	—	1.594	100	(< 1)	(< 1)
53	127	I	1.59	97.7	2.3	5
54	129	Xe	1.507	97.1	2.9	4
—	131	—	1.198	93.3	6.7	8.1
—	132	—	1.449	64.3	35.7	42.3
—	134	—	0.535	89.4	10.6	(< 1)

could induce the downward penetration of protons into the He-rich
layers of an evolved star, as required to fuel s-processing. The
ensuing models are characterized by the formation of
distinctively large reservoirs of protons, up to 5–10 times those
initially suggested in more standard articles on the subject
(Kaeppeler et al., 1990). In contrast, the local concentration of
pollutants, hydrogen primarily, remains very low (see Figure 1
panel i). It is so low, actually, that the subsequent re-ignition of
the H-burning shell, allowing proton captures to occur on the
abundant ^{12}C, can produce ^{13}C, but only minimal traces of ^{14}N
(see Figure 1, panel ii). Under such conditions, the neutrons that are
made available for heavy-element nucleosynthesis by the
^{13}C$(\alpha,n)^{16}$O source are essentially unfiltered by intermediate-
mass nuclei and remain quite abundant.

Three important differences emerge with respect to previous
models.

- First of all, the possibility to synthesize fresh ^{19}F from the
  reactions starting at nitrogen itself is now strongly reduced,
  and the ensuing fluorine abundance predicted as a function
  of metallicity is now in close agreement with actual
  observations (Vescovi et al., 2021).
- A second remarkable implication is the very limited action
  of the so-called *neutron poisons*, i.e., the intermediate-mass
  nuclei with significant cross-sections (^{14}N being their

TABLE 1 (*Continued*) Predictions of the fractional solar abundances from fast and slow *n*-captures (88 ≤ A ≤ 142).

Z	A	Element	N(S.S.)	S.S. r − %	S.S. s − %	AGB s − %
—	136	—	0.435	100	(<1)	(<1)
55	133	Cs	0.368	82.2	17.8	16.7
56	135	Ba	0.300	78.5	21.5	72.2
—	137	—	0.515	41.2	58.8	60.4
—	138	—	3.264	15.8	84.2	91
57	139	La	0.459	21.3	78.7	79.8
58	140	Ce	1.030	13.1	86.9	80.4
—	142	—	0.129	74.9	25.1	14.3
59	141	Pr	0.175	45.4	54.6	66.2

progenitor) acting as filters and limiting the number of neutrons captured by iron and its progeny.

- Finally, a reduced ^{14}N concentration also implies a reduced formation of ^{22}Ne.

This last point follows from the activation of the chain:

$$^{14}\mathrm{N}(\alpha,\gamma)^{18}\mathrm{F}(\beta^{+}\nu)^{18}\mathrm{O}(\alpha,\gamma)^{22}\mathrm{Ne}. \qquad (1)$$
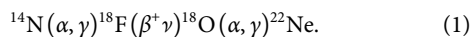
Limiting its efficiency limits the neutron flux that can be released at a higher temperature and with a higher neutron density, when a *thermal pulse* finally develops, accompanied by the sudden enhancement of the He-burning rate (see Busso et al., 1999; Herwig, 2005, for details).

The aforementioned conditions can, in principle, be met by various mixing mechanisms, beyond the MHD one explored here. Some indications in this sense are contained in Appendix 1, where we present some general comments on the stellar models for neutron captures, which are maintained separate from the main text of this article, dedicated to nuclear issues.

We note that the scenario described here for the *s*-process is closer to the classical *phenomenological* approach (Kappeler et al., 1989) than most models discussed in recent years, especially in terms of its generally lower neutron densities, and hence of the operation of reaction branches. As compared to the mentioned models (see e.g., Cristallo et al., 2011), our production of the heavier stable isotopes of neutron-capture elements, like e.g., ^{86}Kr, ^{96}Zr, and ^{100}Pd (see Table 1), is now strongly reduced. This is relevant for our estimates of the Mo isotopes discussed later, where the neutron flow now proceeds mainly along the sides requiring low values of n_n (on average below 10^8 n/cm^3). In this respect, while the ^{22}Ne(α,n)^{25}Mg neutron source (yielding higher neutron densities than the ^{13}C(α,n)^{16}O one) remains important for fixing the operation of reaction branchings, its role is, however, reduced and so is that of IMS, where its activation would be very efficient. As far as one can judge now, super-AGB stars, of mass 8–10 M$_\odot$, currently considered the parents of *e*-capture supernovae (Leung et al., 186 2020), should be at the best
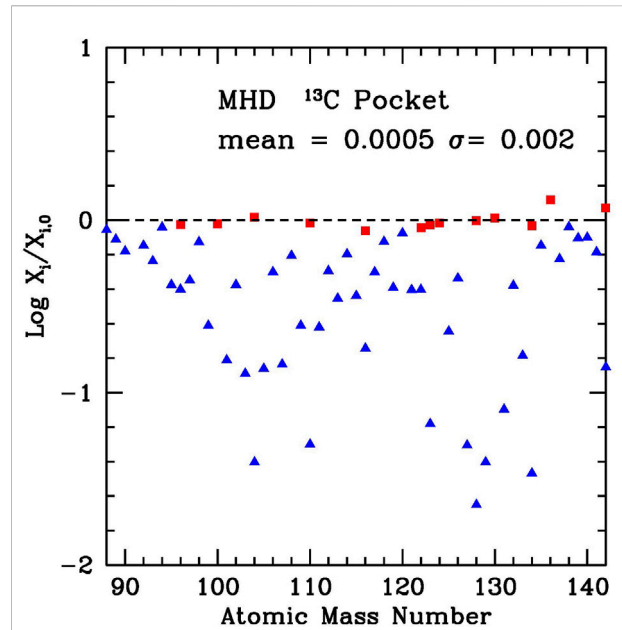

FIGURE 2
Distribution of *s*-process fractional abundances in the mass range 88 ≤ A ≤ 142 considered in the present work, as obtained with the weighting procedure described in Busso et al. (2021) and Palmerini et al. (2021) and (more synthetically) in Section 2. Red symbols refer to the so-called *s−only* nuclei, which are shielded by stable isotopes against contributions from the *r*-process.

marginal in establishing the galactic average of the *s*-nuclei, although they might be relevant in rare, individual cases.

In the computations discussed here, AGB models of the type described so far, extended to stellar masses for 1.3–3 M$_\odot$, with metallicities in the range $-0.8 \leq$ [Fe/H] ≤ 0.1, have been computed for the purposes described in Section 1, using the Kadonis 1.0 cross-section compilation. They were subsequently averaged on galactic time scales with the mentioned choices for the IMF and SFR. The results, expressed in terms of a distribution of abundances for the isotopes in the adopted atomic mass range, were divided by the solar initial concentrations from Lodders (2021) and normalized to unity so that they express average *s*-process contributions to the solar composition. This procedure, aimed at reproducing roughly the outcomes of a galactic chemical evolution model up to the solar formation era, is not exempt from serious drawbacks, which must be taken into account in estimating the global uncertainties. Indeed, while the choices for the IMF and SFR are rather standard, the method cannot account for the real complexity of the inter-relations among the many subsystems of the galaxy. In this respect, the accuracy achieved is roughly at the same level as the one for the *r*-process, described in Section 3; hence, it is adequate for the present purposes. However, in parallel to this, we have, in any case, undertaken a more sophisticated chemo-

dynamical simulation of the galaxy and of its enrichment in *s*-and *r*-isotopes (Antonuccio-Delogu et al., 2022), based on the GIZMO open-source code (see: http://www.tapir.caltech.edu/).

The resulting fractional S.S. abundances in the chosen mass range ($88 \leq A \leq 142$) are shown in Figure 2, adopting the solar composition from Lodders (2021). As discussed previously in various articles (see Trippella et al., 2016; Busso et al., 2021), the results are largely independent of the specific stellar models and type of mixing adopted, provided these consider some general crucial features. These essentially 1) maintain a moderate temperature in the thermal pulses (low mass Kaeppeler et al., 1990); 2) provide a dominant contribution from the $^{13}C(\alpha,n)^{16}O$ reaction (Käppeler et al., 2011); and 3) give rise to mixing mechanisms like those in Figure 1, providing extended ^{13}C distributions with little ^{14}N, to account for the effects on the neutron fluxes mentioned earlier (Liu et al., 2014, 2015; Trippella et al., 2016). By respecting these constraints, in general, one obtains predictions close to 100% for the so-called *s*-only isotopes, where remaining discrepancies can be attributed to nuclear effects. In this respect, given the complexities of stars, it is conceivable that further, non-magnetic, mechanisms suitable to give rise to the same effects might contribute to the picture (see Battino et al., 2016, 2019; Denissenkov and Tout, 2003).

The specific predictions obtained with our models are shown in Figure 2 (where the *s*-only nuclei are indicated in red). There, the reproduction of solar abundances is good, with an average dispersion around 11%. This check gives us a general confidence on the method, allowing us to compare our expectations for the other (non-*s* only) isotopes with the complementary estimates derived from *r*-processing. We then list our model *s*-process contributions to S.S. abundances in Table 1, column 7.

3 The waiting-point model for rapid neutron captures and its results

Since none of the presently discussed scenarios for rapid neutron-capture nucleosynthesis seems to produce a complete S.S. *r*-like pattern, ranging from the light trans-Fe region up to the actinides, for this study (i.e., for comparing the isotopic abundance fractions of the *s*-process and *r*-process in the S.S. composition), we decided to choose an updated version of the classical site-independent *waiting-point* concept (Coryell, 1956; Burbidge et al., 1957; Cameron, 1957; Kratz, 1988; Kratz et al., 1993). It assumes a chemical equilibrium between fast neutron captures (n, γ) and photo-disintegrations (γ, n) within isotopic chains, followed by a β-equilibrium during the freeze-out phase within isobaric chains. In our present approach, we combine the results from our early publications (see Kratz et al., 1993) with the later improvements from experimental data and microscopic models (see Pfeiffer et al., 1997; Kratz et al., 2000; Möller et al., 2003; Farouqi et al., 2010; Kratz et al., 2014, Kratz et al., 2019).
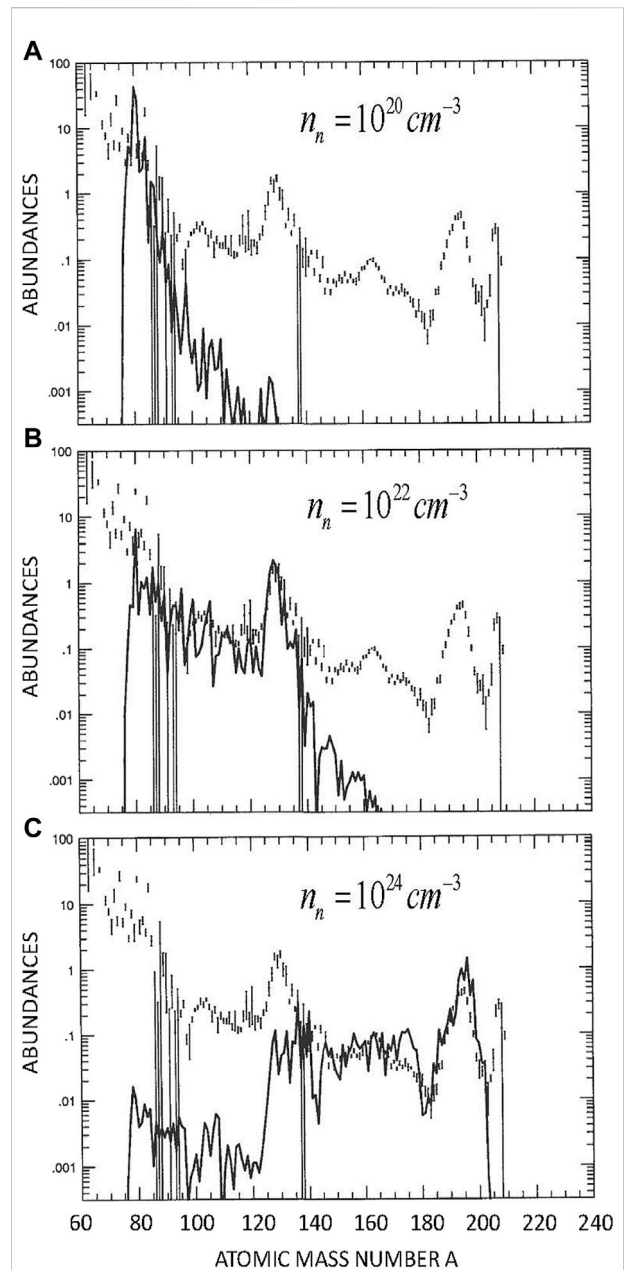

FIGURE 3
Results of time-dependent steady-flow *r*-process calculations with neutron densities $n_n = 10^{20}$ cm^{-3} **(A)**, $n_n = 10^{22}$ cm^{-3} **(B)**, and $n_n = 10^{24}$ cm^{-3} **(C)**, and corresponding process duration $\tau_r = 1.2$, 1.7, and 2.1 s, respectively. The abundances by number are shown in the figure, in a scale in which $N(Si) = 10^6$. This is compared to the S.S. *r*-" residuals" in the same scale. In principle, adding up the abundances of those three *r*-process components will result in the complete S.S. *r*-process abundance blend (adapted from Kratz et al., 2000).

As an example of the *r*-process abundances we had obtained already two decades ago, in Figure 3, we show the results from three specific waiting-point calculations with different neutron densities and corresponding process duration (solid lines), in

comparison to the S.S. *r*- "residuals" from that time. In these calculations, the global deformed *Extended Thomas Fermi Model plus Strutinsky integral* and the *Bogolyubov-enhanced shell-quenching*, (*ETFSI-Q*) mass model (Pearson et al., 1996) have been used, together with the corresponding *Quasi-particle random-phase approximation* for *Gamow-Teller and first forbidden* transitions (*QRPA(GT + FF)*) (see Pfeiffer et al., 2002; Möller et al., 2003). We show here these exemplary results because, while documenting the importance of the $N = 50$, 82, and 126 bottlenecks of the *r*-matter flow, they are completely site-independent and, despite this, they already show the general *r*-abundance patterns of the different *r*-process scenarios, more or less as we know them today and as we have published later in Farouqi et al. (2010) and Kratz et al. (2014).

In the first panel of Figure 3, a low neutron density $n_n = 10^{20}$ cm^{-3} and a process duration of $\tau_r = 1.2$ s were chosen to obtain a "best fit" of the $A \simeq 80$ *r*-process peak from its known $N \simeq 50$ precursor isotopes between $Z = 29$ (Cu) and $Z = 32$ (Ge) (see Kratz et al., 1991). Beyond this peak, a steeply decreasing abundance pattern by about four orders of magnitude is observed for the mass region above, down to the minimum yields at $A \simeq 130$. Currently, we know that this pattern "mimics" the isotopic distributions of Sr, Zr, Mo, and Ru observed in the presolar SiC grains of type *X*, measured by the Argonne–Chicago group (see Pellin et al., 2006; Farouqi et al., 2009; Kratz et al., 2019). The nucleosynthesis origin of this abundance pattern up to the rising wing of the second *r*-process peak at $A \simeq 130$ has been attributed to classical *ccSNe* (Kratz et al., 1993; Farouqi et al., 2009, 2022). The second panel of Figure 3 shows an abundance component obtained with a slightly higher neutron density of $n_n = 10^{22}$ cm^{-3} and a process duration of $\tau_r = 1.7$ s. It covers the S.S. *r*-region up to the full $A \simeq 130$ peak and continues with decreasing abundances in the light *R.E.E* region up to about Eu. This *r*-process component has been normalized to the *r*-only isotopes ^{128}Te and ^{130}Te, where again a number of experimental data for the progenitor isotopes from $Z = 47$ (Ag) up to $Z = 51$ (Sb) exist (see Kratz et al., 2000).

In addition to the $A \simeq 130$ *r*-abundance peak, a wide range of (β, γ) and delayed neutron spectroscopic data, as well as accordingly updated microscopic models, are available in the region near $Z = 34$ (Se) and $Z = 40$ (Zr), where the shape transition between the magic $N = 50$ shell *via* the spherical $N = 56$ subshell up to the onset of strong (rigid rotor) ground-state deformation plays a decisive role in the determination of various nuclear properties (see Kratz et al., 1983a,b; Lhersonneau et al., 1994; Möller et al., 2003). As an example, the improved understanding of the nuclear structure resulted in changes of theoretical β-decay properties for the $N \simeq 56$ isotopes by factors from 13 (e.g., for ^{89}Se) up to 53 (e.g., for ^{93}Sr). Fast neutron captures dominant in this regions above $A \simeq 90$ (our second n_n component) are frequently denoted as the *weak r-process*. Today, we know that its abundance pattern "mimics" the elemental
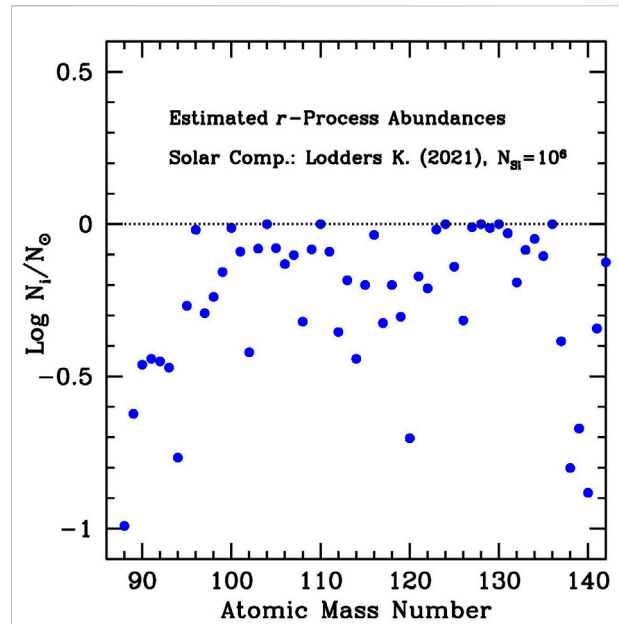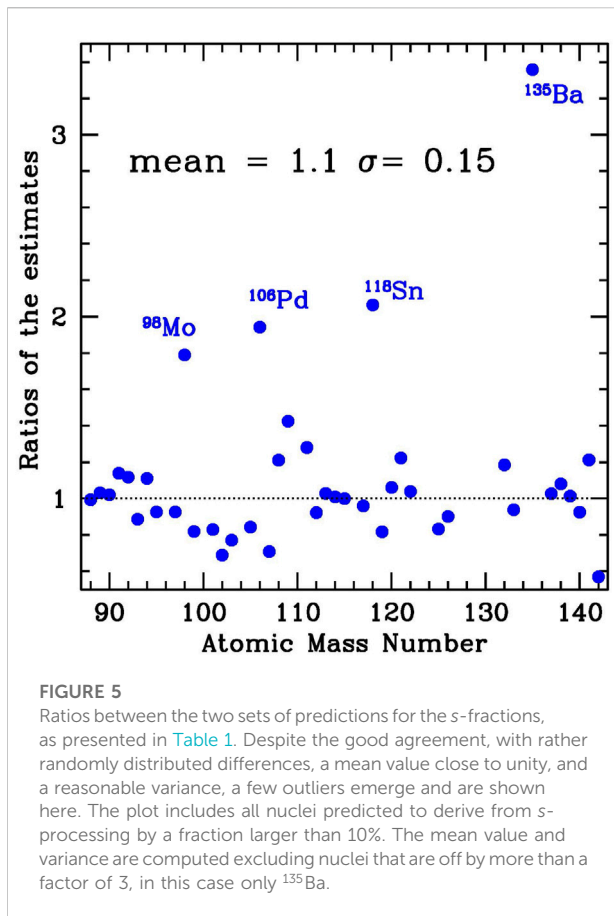

FIGURE 4
Distribution of *r*-process fractional abundances as estimated by our *waiting-point* approximation, according to the discussion in the text. Similar to what is shown in Figure 2 for the *s*-process, nuclei considered to be of essentially pure *r*-process origin ($\geq 95\%$) are indicated with red symbols. It should be noted that, following a common habit, the second *r*-peak was normalized to ^{128}Te and ^{130}Te, assumed to be *r*-only. This has some support in the data of Table 1, column 7, where we show that, even in the estimates from AGB models, their *s*-fractions are predicted to be ≲1%.

distribution of metal-poor, *r-poor*, or *incomplete r* stars with [Eu/Fe] ≲ 0.2.

A typical example of such a type of star is the so-called "Honda star" (HD122563, see Honda et al., 2007), with its overabundances relative to the S.S. *r*-pattern of the light trans-Fe elements and its decreasing abundances in the rare earth element (*R.E.E.*) region between $Z = 68$ (Er) and $Z = 70$ (Yb). As one of the signatures to classify the different types of halo stars, astronomers use, for example, the abundance ratio of light-to-heavy mass regions, using $Z = 38$ (Sr) and $Z = 63$ (Eu) as representative elements. For the *r*-poor Honda star, the ratio (Sr/Eu) ≃ 505, which is a factor 24, higher than the S.S. *r*-ratio of 21. The nucleosynthesis origin of these *r*-poor stars can very likely be attributed to *jet-like* or *magneto-rotational* SNe, with low strengths of magnetic fields and of rotation (see Nishimura et al., 2017; Farouqi et al., 2022).

The third panel in Figure 3 shows a typical abundance pattern for a *main r-process* component, with consequently higher neutron densities (here, $n_n = 10^{24}$ cm^{-3}) and slightly longer process duration (here, $\tau_r = 2.1$ s), which covers the S.S. *r*-region of the *R.E.E.*, the full third *r*-process peak at $A \simeq 195$ and beyond, up to the actinides. This last n_n component has

FIGURE 5
Ratios between the two sets of predictions for the *s*-fractions, as presented in Table 1. Despite the good agreement, with rather randomly distributed differences, a mean value close to unity, and a reasonable variance, a few outliers emerge and are shown here. The plot includes all nuclei predicted to derive from *s*-processing by a fraction larger than 10%. The mean value and variance are computed excluding nuclei that are off by more than a factor of 3, in this case only ^{135}Ba.

been normalized to the top of the peak with its *r*-only isotopes of Os, Ir, and Pt, formed in the back decay of their extremely neutron-rich, experimentally still unknown, $N \simeq 126$ precursor isotopes of the nuclei from $Z = 68$ (Er) to $Z = 72$ (Hf). Presently, we know that this kind of a *main* or even *strong r-process* pattern "mimics" the elemental abundances of the so-called *r*-enriched metal-poor halo stars with [Eu/Fe] $\geq +0.8$. Typical examples for this class of stars are the normal *r-II Sneden star* (CS22892-052, see Sneden et al., 2003) and the so-called *actinide-boost Cayrel-star* (CS31082-001, see Hill et al., 2002), attributed to different types of *NSM* (see Rosswog et al., 2018; Farouqi et al., 2022).

By simply adding up these three abundance patterns, we get a total abundance distribution which comes relatively close to the S.S. *r-blend*. In particular, our computed estimates for the *r*-process contributions to S.S. abundances, normalized to N(Si) = 10^6, and with updated nuclear inputs are presented in Figure 4.

In the simplest possible physical realization of the solar *r*-process distribution, stellar and *NSM* models would have to find where exactly the aforementioned "components" are produced by nucleosynthesis models. Quite obviously, this is a very naive view, as no astrophysical source can be imagined to host such simple neutron-capture processes at constant neutron density. The previous indications, and their descending suggestions for

nuclear parameters, have instead to be looked at as first-order approximations, good for an assessment of the very complex nuclear problems related to the reaction paths of *r*-nuclei. As we shall see, even this simple approach already yields useful indications and a remarkable general consistency with Solar System data. Also attributing the aforementioned components to specific stellar sources is a difficult task in the cluster abundance patterns observed in galactic, mainly low-metallicity, stars. With these limits in mind, we comment, however, briefly on this point in Appendix 1.

4 Comparisons and discussion

A comparison of the results from the two neutron-capture approaches outlined so far (Figures 2, 4) is presented in Table 1. As mentioned, for what concerns the *r*-process model, here the original computations shown in Figure 3 have been updated, considering various different mass models with consistent *QRPA(GT + ff) β*-decay predictions by Farouqi et al. (2010) and the quoted recent deformed *FRDM12/QRPA* model combination by Kratz et al. (2014).

In Figure 5, we show the resulting ratios between the two sets of expectations for the *s*-process fractions of solar abundances. The agreement between these completely independent approaches is quite good. It is actually the best so far published, to our knowledge.

Despite this satisfactory outcome of our work, some discrepancies remain and require a more detailed analysis, as presented in the following subsections.

4.1 ^{98}Mo

The element Mo as measured in early S.S. materials provides important tools for understanding the contamination of the presolar nebula in heavy nuclei. On the one hand, its isotopic admixture in the *mainstream*-type of presolar SiC grains (Stephan et al., 2019) is quite typical of AGB star progenitors (Palmerini et al., 2021). On the other hand, Mo isotopes show very different anomalies in the so-called presolar *SiC – X*-grains (Pellin et al., 2006), whose origin has been attributed to *ccSNe* (Farouqi et al., 2009; Kratz et al., 2019).

Stephan and Davis (2021) inferred, from isotopic measurements in presolar SiC grains of AGB origins, estimates for the *r*- and *s*-process decoupling of Mo isotopes. In the specific case of ^{98}Mo, our estimates from the *waiting-point* approximation would suggest a lower *s*-process percentage (42.3%) than the one from the aforementioned authors (74.4%, very similar to the expectation from AGB models, 75.7%). In *s*-process scenarios, the synthesis of lighter Mo isotopes depends on several branching reactions at Nb isotopes, with contributions from isomeric states at ^{93}Nb,

[94]Nb, and [95]Nb (see Figure 5 in Palmerini et al., 2021). All of them terminate before [96]Mo, which is an *s*-only nucleus whose abundance is very well reproduced by the models discussed in Section 2 (see Figure 2). We remember, however, that cross-sections in the Zr–Mo region are still very uncertain (for the unstable [95]Zr, experimental information is essentially missing), and new measurements are crucial here for any conclusion. Cross-sections for Mo isotopes are actually under measurement now by the n_TOF collaboration (Guerrero et al., 2013).

Concerning the *r*-process predictions, we compare the results from the old mass- and shell model combination *ETFSI-Q/QRPA* (as used e.g., in Kratz et al., 2000) with our most recent *FRDM/QRPA* computations (see e.g., Kratz et al., 2014). For both model combinations, the basic nuclear parameters are obtained from the mass model. They are the mass derivatives Q_β and S_n, in addition to the ground-state shape of the β-decay mother isotope, related to the *quadrupole deformation parameter*, ϵ_2, (for which positive values mean prolate shapes and negative values mean oblate shapes). With these parameters, the so-called *β-strength function* is calculated within the *QRPA* shell model, from which spins and parities (J^π), level schemes, β-feedings (log *ft* values), and finally the integral quantities, $T_{1/2}$ and β-delayed neutron-branchings P_{xn}, are deduced.

To summarize, for [98]Mo and the following cases [118]Pd, [118]Sn, and [135]Ba, we compare the respective hold-up points of the isotopic *r*-matter flow at $S_n \lesssim 2$ MeV for masses A and $(A+1)$, which define the *r*-process progenitor isotopes with their β-decay parameters $T_{1/2}$ and P_{xn} and their resulting initial isotopic waiting-point abundances. After modulation by the β-delayed *n*-branchings during the freeze-out, the final abundance yields of the stable nuclei of interest are obtained.

For the specific case of [98]Mo ($Z = 42$, $N = 56$), in both mass/shell model combinations, the dominant progenitors at $A = 98$ are [98]Kr ($Z = 36$, $N = 62$) and [98]Se ($Z = 34$, $N = 64$). For the *ETFSI-Q/QRPA* version, they account for $\simeq 81\%$ and $\simeq 19\%$, respectively. The S_n values for the dominant [98]Kr hold-up point are practically identical for both model combinations, and (to our relief) the β-decay properties $T_{1/2}$ and P_n are experimentally known for the whole isobaric decay chain to [98]Mo. Since the relevant nuclear data predictions for [98]Se are also quite similar, we can estimate the total effect for $A = 98$, which is negligible.

More substantially, instead, the effect from the single waiting-point progenitor isotope in the $A = 99$ mass chain ($Z = 35$, $N = 64$), i.e., [99]Br will feed the $A = 98$ mass chain *via* its predicted high P_n value. Here, relative to *ETFSI-Q*, in the *FRDM12* mass model, the decreasing S_n trend to the hold-up isotopes with $S_n \simeq 2$ MeV is shifted by two units to higher masses. As a consequence, with the *FRDM/QRPA* model combination, the calculated waiting-point abundance of [99]Br is reduced. In addition, taking into account the slightly different P_n predictions, the final S.S. *r*-fraction of the stable isotope [98]Mo would be reduced from 57.7%, as listed in Table 1, to about 45%, which

would correspond to an increase of the S.S. *s*-fraction from 42.3% to about 55%, in better agreement with the AGB s-process model predictions, now being only a factor 1.38 lower than the S.S. *s*-values.

The aforementioned discussion is only an attempt of clarifying how the present numbers still have an unavoidable *local* dependence on the choice of nuclear input data. We underline that these difficulties cannot be overcome by referring to specific astrophysical sites, being rooted in the nuclear inputs; they will affect equally any nucleosynthesis model, as all such models require nuclear input parameters. Our estimates represent, therefore, a *reasonable* approximation to the present state-of-the art. Although a "universal" set of inputs does not exist, we can, nevertheless, receive useful indications from comparisons like the ones discussed here.
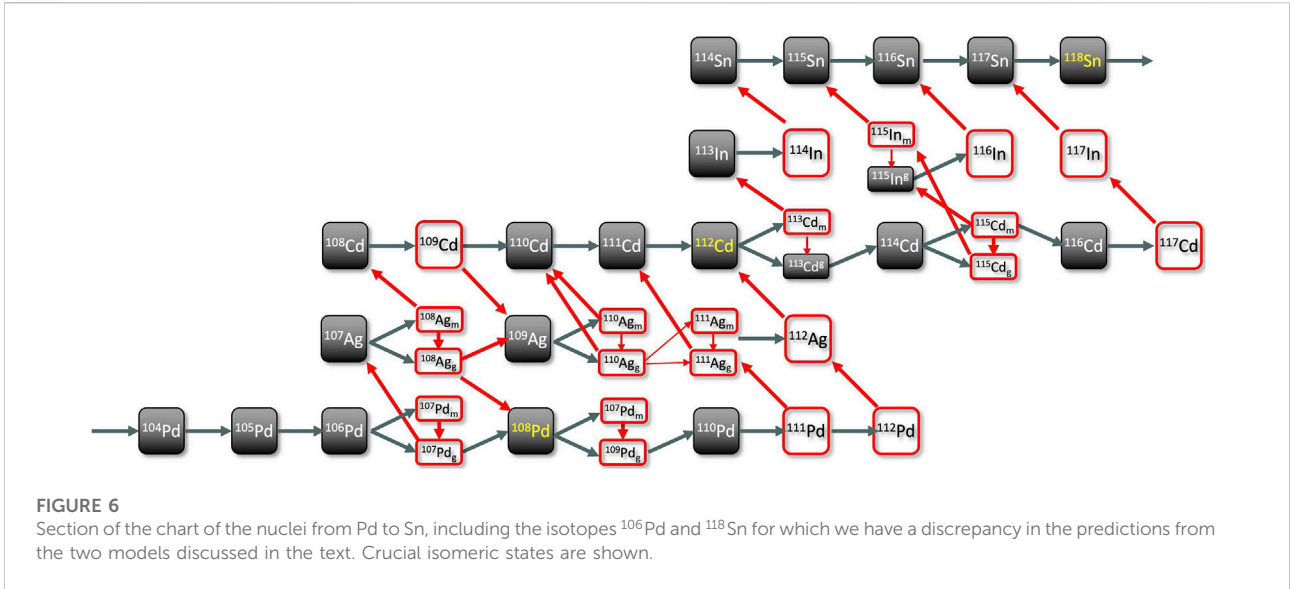
4.2 [106]Pd and [118]Sn

A very complex situation characterizes the region from Pd to Sn, for which the rather intricated *s*-process branching points are illustrated in Figure 6.

In the past 15 years, this region was the subject of a hot debate on the possible existence of a *light element primary production* mechanism, or *LEPP* (Travaglio et al., 2004), just devised to explain abundance deficiencies in this mass region (Montes et al., 2007). Today little remains of that debate, with the understanding that a blend of different *r*-process components is required (see Figure 3 and Farouqi et al., 2009).

Even now, however, the outliers [106]Pd and [118]Sn certify the difficulties in this mass interval. From the *s*-process point of view, the cross-sections to the various (not always thermalized) isomeric states (Theis et al., 1998) shown in Figure 6 are almost unknown or very uncertain, as is the behavior of the branching β-decays in the stellar plasma. This is, therefore, an atomic mass zone where new experimental studies are needed, both for cross sections and decay rates, before the estimates of Table 1 can be improved significantly. Among the β-decay rates to measure in highly ionized environments, we underline, in particular, the cases of [113,115]Cd and [115]In, hosting possibly non-thermalized isomeric states (Takahashi and Yokoi, 1987).

From the *r*-process point of view, for the even–even nucleus [106]Pd ($Z = 46$, $N = 60$), the nuclear data analysis starts to become more difficult than the possible *r*-process progenitor isotopes of lighter elements. There are two main reasons for this. First, the strongly dominating, single *r*-process precursor isotope ($Z = 38$, $N = 68$) [106]Sr was not known when the *ETFSI-Q/QRPA* and *FRDM/QRPA* calculations were performed. Some β-decay properties were, however, already known from the neighboring Y to Nb isotopes, which could be used to check the reliability of the model predictions for [106]Sr, and second, these progenitor sites already have two neutrons beyond the $N = 66$ mid-shell, between the magic $N = 50$ and $N = 82$ shells, where

FIGURE 6
Section of the chart of the nuclei from Pd to Sn, including the isotopes ^{106}Pd and ^{118}Sn for which we have a discrepancy in the predictions from the two models discussed in the text. Crucial isomeric states are shown.

the transition between strongly deformed and spherical shapes is beginning. As expected for $N = 68$, both model combinations still predict a strong ground-state deformation of $\epsilon_2 \simeq 0.3$. Hence, the resulting patterns of the β-strength functions should also be quite similar. However, a first difference is already observed for the nuclear mass derivatives Q_β (energy output of the decay) and S_n (binding energy of the last neutron). The old mass formula *ETFSI-Q* predicts a 1.75-MeV larger Q_β value and a 230 keV lower S_n value relative to the more modern *FRDM* model. Consequently, the theoretical $T_{1/2,FRDM}$ is larger (by a factor $\simeq$ 2.3), and the $P_{n,FRDM}$ is reduced (by a factor $\simeq 1.5$). By combining the possible effects of these two nuclear quantities, the final result on the S.S. *r*-fraction will be negligible.

For the predicted trends of the theoretical S_n values, the situation is, however, different. For the *FRDM* model, the hold-up point of the *r*-matter flow in the Sr isotopic chain at $S_n \simeq$ 2 MeV will again be slightly shifted to higher masses, as compared to the *ETFSI-Q* prediction. According to the nuclear Saha equation, this will distribute the initial waiting-point abundances to some extent to the progenitors ^{106}Sr and ^{108}Sr. A rough estimate of the likely effect on the final S.S. *r*-fraction would result in its reduction from $\simeq 74\%$ from the *ETFSI-Q/QRPA* approach to values between $\simeq 67\%$ and $\simeq 59\%$. This would reduce the present "discrepancy" in the latter case from a factor 1.5 to around 1.2.

Again, the ($Z = 50$, $N = 68$) even–even isotope ^{118}Sn has only a single, strongly dominating (but experimentally completely unknown) *r*-process progenitor ($Z = 42$, $N = 76$), i.e., ^{118}Mo. Furthermore, this isotope lies in the second part of the shape-transition region, only six neutrons below the spherical $N = 82$ shell, where practically all global mass models, not only *ETFSI-Q* and the different *FRDM* versions, have severe difficulties to predict reliable nuclear structure trends.

According to the aforementioned analysis presented, one can say that, in this mass range, future improvements of the agreement between the *r*-process and *s*-process models can possibly come from revisions of the nuclear parameters (cross sections and, probably more important, β-decay rates) for the slow neutron captures. Concerning the *r*-process, because of its "exponential sensitivity" (Saha equation), we would primarily request new S_n (nuclear mass) revisions and only as a second priority estimates of β-decays far from stability.

4.3 ^{135}Ba

The *s*-process production of ^{135}Ba remains very uncertain today, as a consequence of the evidence that the decay rates of Cs isotopes adopted for decades (Takahashi and Yokoi, 1987) are not accurate enough. Revisions have been recently presented (Li et al., 2021; Taioli et al., 2021) and thanks to them, it was shown that it is now possible to improve considerably both the reproduction of solar abundances for the *s*-only nuclei ^{134,136}Ba (see Busso et al., 2021; Taioli et al., 2021) and the isotopic admixture of Ba isotopes in presolar SiC grains (Li et al., 2021; Palmerini et al., 2021). However, our estimate for the *s*-contribution to ^{135}Ba still depends remarkably on other issues. This includes, primarily, the cross sections of the same Ba isotopes and of ^{133}Cs, then also the details on how the ^{134}Cs($\beta^+\nu$)^{134}Ba and ^{135}Cs($\beta^+\nu$)^{135}Ba operate in stars, which require the precise knowledge of the temperature evolution in the layers where ^{135}Ba is produced, i.e., the convective *thermal instabilities* of the He-shell in AGB stars (Busso et al., 1999). Ultimately, this is linked to how we model convection; hence, here we cannot absolutely mention that the remaining uncertainties are purely nuclear in origin. As shown in

Figure 13a of Palmerini et al. (2021), even the most precise constraints available currently (i.e., those from the isotopic Ba admixture in mainstream presolar SiC grains) still offer ample space for a possible lower s-process contribution to this nucleus, which would fit better with the r-process predictions (see Table 1, column 6, and Figure 5. See also the following discussion).

Let us then see whether the origin of the discrepancy in Table 1 and in Figure 5 for ^{135}Ba can come from uncertainties in the r-process approach. The potential progenitor isotopes at $Z = 49$ (In) and up to $Z = 51$ (Sb) are situated in a shape transition region, in this case between the spherical $N = 82$ shell closure and the well-known strongly deformed $R.E.E.$ region beyond $N \simeq 90$.

According to our two model combinations, the three dominating precursor isotopes that may contribute to the abundance of ^{135}Ba are ^{135}In ($Z = 49$, $N = 86$), ^{136}Sn ($Z = 50$, $N = 86$), and ^{138}Sn ($Z = 50$, $N = 88$). Since these isotopes are predicted to have still spherical ground-state shapes ($\epsilon_2 \lesssim 0.1$), they should have quite similar nuclear mass and β-decay rate values. However, since the r-progenitor nuclei lie already quite far from β-stability, their β-delayed neutron-branchings of one to three neutrons play an important role. This is, indeed, confirmed by the available experimental data (Audi et al., 2012), which indicate a clear preference for the $FRDM12/QRPA$ model predictions as compared to the older $ETFSI$-$Q/QRPA$ approach.

In any case, both model combinations agree on the fact that, in the rather complex β-delayed neutron-branchings during the decay back to stability of both progenitor nuclei ^{135}In and ^{138}Sn, only negligible fractions of the initial abundances reach ^{135}Ba. Hence, only the β-delayed neutron decay of the progenitor ^{136}Sn finally populates ^{135}Ba, with about 40% of its initial abundance. Due to the complex β-delayed neutron decay pattern far from stability, the resulting effect of only a slight reduction in the final S.S. r-fraction of ^{135}Ba (maybe by $\simeq 10\%$) can be inferred.

An indication of what should be obtained here for ^{135}Ba can be obtained from observations of r-II metal-poor stars, through the Ba $- f_{odd}$ parameter. In the isotopic composition of Ba of a certain environment, Ba $- f_{odd}$ expresses the abundance ratio of odd isotopes to the total abundance of the element. Under r-process conditions, this last can be approximated by excluding the even isotopes, except for the dominant ^{138}Ba so that

$$Ba - f_{odd} \simeq \frac{^{135}Ba + ^{137}Ba}{^{135}Ba + ^{137}Ba + ^{138}Ba}. \qquad (2)$$

Ba $- f_{odd}$ can be measured by high-resolution spectroscopy in a number of metal-poor halo stars (see Mashonkina and Christlieb, 2014; Mashonkina and Belyaev, 2019, and Mashonkina et al., 2017, private communication) by a careful analysis of the hyperfine splitting. From these observations, a mean value of Ba $- f_{odd} = 0.4 \pm 0.10$ was obtained.

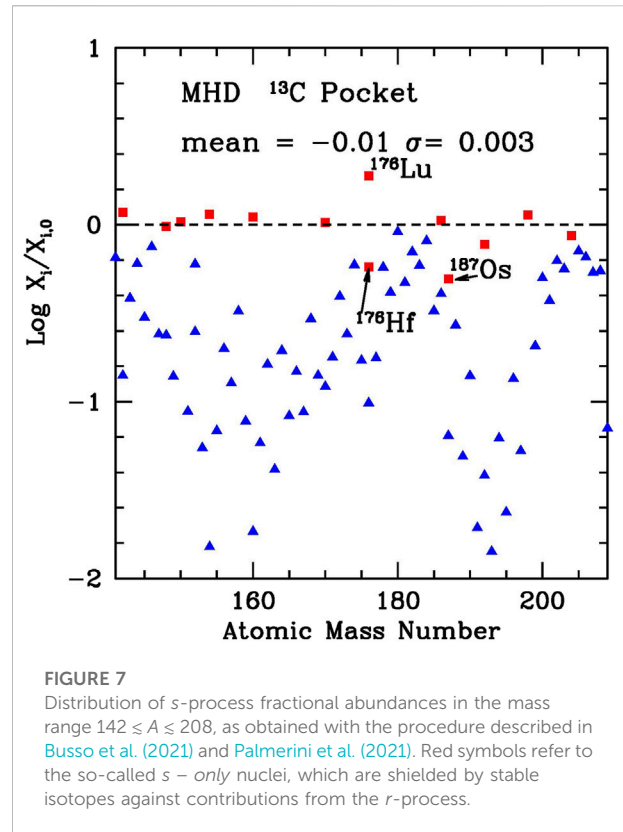This result can now be compared to that of our model predictions. From the data of $ETFSI$-$Q/QRPA$ (Kratz et al.,

FIGURE 7
Distribution of s-process fractional abundances in the mass range $142 \lesssim A \lesssim 208$, as obtained with the procedure described in Busso et al. (2021) and Palmerini et al. (2021). Red symbols refer to the so-called $s - only$ nuclei, which are shielded by stable isotopes against contributions from the r-process.

2007), a mean value of 0.49 $\pm$ 0.03 could be derived, while from the more recent $FRDM12/QRPA$ version (Kratz et al., 2014), a somewhat lower mean value of 0.43 $\pm$ 0.03 was obtained. From Table 1, we would now get $\simeq 0.45$. These results are all in good agreement with the Ba $- f_{odd}$ measurements in halo stars. On the contrary, from our AGB s-process estimates shown in Table 1, the resulting value is Ba $- f_{odd} \lesssim 0.3$, dominated by the estimate for ^{135}Ba.

These facts suggest that in this case, it is the s-process computation that might be improved by new nuclear data on cross sections and decay rates. For the weak interactions, in particular, experimental measurements in ionized plasmas on the rates for the β^- decays of ^{134,135}Cs would be highly needed.

4.4 Nuclei heavier than A = 142

Our estimates for S.S. abundances of heavy nuclei ($A \geq 142$) as descending from the AGB models adopted in the present study are shown in Figure 7. As is clear from the plot, over a general trend characterized by a good reproduction of the solar abundances for s-only nuclei (red dots), with a small dispersion, three very remarkable outliers appear, at ^{176}Lu, ^{176}Hf, and ^{187}Os, which are among the reasons why we did not attempt a complete comparison in this mass range.

The outliers of Figure 7 are related to nuclear problems known since a long time and for which only new measurements of decay rates under partial ionization conditions would help. For the isotopes ^{176}Lu and ^{176}Hf, a thorough analysis was performed by Wisshak et al. (2006a); Wisshak et al. (2006b), to which we address interested readers. Here, isomeric states at ^{175}Yb, ^{176}Lu, and ^{177}Hf are involved in the reaction chain. While for ^{175}Yb and ^{177}Hf, the isomers are depopulated, and the nuclei are in their ground states under s-process conditions, this is not so for ^{176}Lu. Its ground state is essentially stable ($T_{1/2} \simeq 3.8 \times 10^{10}$ yr) and was considered for a long time as a clock for cosmo-chronology (Audouze et al., 1972). Instead, it is now known that the isomer is partially thermalized at the temperature ($T \simeq 23$–25 keV) of AGB thermal pulses. This induces a sharp reduction of the half-life due to the high-energy thermal photons. As a consequence, ^{176}Lu becomes, in principle, a sensitive thermometer of the environment. For this to occur, however, all the pertinent cross sections and decay rates should be well-known. On the contrary, for the parent ^{175}Yb, only theoretical estimates exist, for both parameters, and measurements for ^{176}Lu itself were carried out in Karlsruhe (Wisshak et al., 2006a) and are waiting for more modern confirmations. Also, the ^{176}Hf destruction, through neutron captures either to ^{177}Hf^g or to ^{177}Hf^m should in this context be verified. High accuracy is required to settle this problem, as the decay of ^{176}Lu was traditionally assumed to control the ^{176}Hf abundance (Prantzos, 2019), which is, in general, difficult to achieve, as the solar abundance of Hf is larger than that of Lu.

Another crucial issue concerns ^{187}Os. Its parent ^{187}Re is a very long-lived nucleus at low temperatures ($T_{1/2} \simeq 43.5$ Gyr). However, it is known that under stellar conditions, this isotope, like, e.g., ^{207}Tl and ^{163}Dy (which is stable at laboratory temperatures), can undergo *bound* state decays, i.e., decays where the electron is not emitted as a free particle but is captured by the daughter nucleus (^{187}Os in this case) to form a hydrogenoid bound state. This significantly increases the decay rate, (by nine orders of magnitudes for completely stripped ^{187}Re), as verified, e.g., by works at the ESR storage ring in Darmstadt (Bosch, 2006; Litvinov and Bosch, 2011). Plasma traps like the future *PANDORA* experiment (Mascali et al., 2020) will soon offer a place where to mimic the partial ionization conditions prevailing in AGB stars, providing new information on several uncertain β-decay rates mentioned in this article for the s-process.

5 Preliminary conclusions and expected improvements

In this study, we present predictions for the contributions to solar abundances of trans-Fe nuclei synthesized by neutron captures. Both the r-process estimates and the complementary s-process ones are shown, in the aim of clarifying the problems that are still affecting their respective nuclear inputs. We limited our analysis to the atomic mass range between Sr and Pr because

for heavier nuclei, both models are affected by rather large uncertainties, making such a comparison difficult. In the two independent views, we adopted approaches that are already satisfying basic, universally recognized constraints so that we can trust that the remaining inconsistencies do not come from astrophysical model details but can be traced back to limits in the available nuclear ingredients.

The results are shown in terms of independent predictions for the s-process fraction of solar abundances and demonstrate an unprecedented agreement, where in the majority of cases, the ratios of the two estimates are ≲ 1.20 (a 20% scatter), not far from the uncertainty of the experimental σN curve. For four nuclei (^{108}Mo, ^{106}Pd, ^{118}Sn, and ^{135}Ba), there is a clear disagreement that requires a critical analysis. From the ensuing discussion, it has been suggested that decay rates crucial for the s-process (in particular at ^{113,115}Cd, ^{115}In, and ^{134,135}Cs) be verified experimentally, especially in ionized plasma environments. Although, as mentioned, we did not perform a detailed comparison for the R.E.E., from a simple inspection of the existing problems in reproducing s-only nuclei, the same conclusion emerges for some heavy nuclei that are very long-lived in the laboratory but display a different behavior in the high-temperature and high-ionization conditions of a stellar plasma (these are e.g., the cases of ^{176}Lu and ^{187}Re).

From the r-process point of view, of course, the situation is much more difficult. In the ideal case, one would request experimental data for r-process progenitor isotopes related to nuclear masses (in particular neutron-separation energies, S_n and β-decay properties, $T_{1/2}$, and P_{xn}). Ionic traps like *Pandora* will have, however, no access to this data region because of significantly short terrestrial half-lives (for the most important neutron magic isotopes, except ^{80}Zn, $T_{1/2} \lesssim 200$ ms).

For the R.E.E. nuclei and the Pt-peak, actually, progenitor isotopes lie very far from stability and are in most cases out of any experimental reach, even for facilities like *RIKEN* or *CERN/ISOLDE*. We should then focus on the nuclear structure development within isobaric chains, from stability toward the progenitor nuclei, in order to derive more reliable, local, and short-range extrapolations.

For lighter nuclei, whenever possible, detailed $1n$- to $3n$-branchings should be measured, for isotopes involved in the β-decay back to stability. Of particular interest, in this case, are nuclides at magic and semi-magic neutron shells (which act as bottlenecks for the r-process matter flow), as well as isotope sequences in the different shape-transition regions, where practically all global models have large uncertainties.

Data availability statement

The original contributions presented in the study are included in the article/Supplementary Material; further inquiries can be directed to the corresponding author.

Author contributions

MB: conceptualization, computations, and text writing. K-LK: conceptualization, computations, and text writing. VA-D: conceptualization and computations. SP: conceptualization and computations. WA: conceptualization and computations.

Funding

Acknowledgments

Conflict of interest

The authors declare that the research was conducted in the absence of any commercial or financial relationships that could be construed as a potential conflict of interest.

Publisher's note

All claims expressed in this article are solely those of the authors and do not necessarily represent those of their affiliated organizations, or those of the publisher, the editors, and the reviewers. Any product that may be evaluated in this article, or claim that may be made by its manufacturer, is not guaranteed or endorsed by the publisher.

References

Abbott, B. P., Abbott, R., Abbott, T. D., Acernese, F., Ackley, K., Adams, C., et al. (2017). GW170817: Observation of gravitational waves from a binary neutron star inspiral. *Phys. Rev. Lett.* 119, 161101. doi:10.1103/PhysRevLett.119.161101

Antonuccio-Delogu, V., Busso, M., and Palmerini, S. (2022). Beyond Iron: Numerical models of s- and r-process element distributions. *Universe* (in press).

Audi, G., Kondev, F. G., Wang, M., Pfeiffer, B., Sun, X., Blachot, J., et al. (2012). The Nubase2012 evaluation of nuclear properties. *Chin. Phys. C* 36, 1157–1286. doi:10.1088/1674-1137/36/12/001

Audouze, J., Fowler, W. A., and Schramm, D. N. (1972). ^{176}Lu and s-Process Nucleosynthesis. *Nat. Phys. Sci.* 238, 8–11. doi:10.1038/physci238008a0

Battino, U., Pignatari, M., Ritter, C., Herwig, F., Denisenkov, P., Den Hartogh, J. W., et al. (2016). Application of a theory and simulation-based convective boundary mixing model for AGB star evolution and nucleosynthesis. *Astrophys. J.* 827, 30. doi:10.3847/0004-637X/827/1/30

Battino, U., Tattersall, A., Lederer-Woods, C., Herwig, F., Denissenkov, P., Hirschi, R., et al. (2019). NuGrid stellar data set - III. Updated low-mass AGB models and s-process nucleosynthesis with metallicities Z= 0.01, Z = 0.02, and Z = 0.03. *Mon. Not. R. Astron. Soc.* 489, 1082–1098. doi:10.1093/mnras/stz2158

Bisterzo, S., Gallino, R., Käppeler, F., Wiescher, M., Imbriani, G., Straniero, O., et al. (2015). The branchings of the main s-process: Their sensitivity to α-induced reactions on ^{13}C and ^{22}Ne and to the uncertainties of the nuclear network. *Mon. Not. R. Astron. Soc.* 449, 506–527. doi:10.1093/mnras/stv271

Bisterzo, S., Gallino, R., Straniero, O., Cristallo, S., and Käppeler, F. (2012). The s-process in low-metallicity stars - III. Individual analysis of CEMP-s and CEMP-s/r with asymptotic giant branch models. *Mon. Not. R. Astron. Soc.* 422, 849–884. doi:10.1111/j.1365-2966.2012.20670.x

Bisterzo, S., Travaglio, C., Gallino, R., Wiescher, M., and Käppeler, F. (2014). Galactic chemical evolution and solar *s*-process abundances: Dependence on the^{13}c-pocket structure. *Astrophys. J.* 787, 10. doi:10.1088/0004-637X/787/1/10

Bosch, F. (2006). Beta decay of highly charged ions. *Hyperfine Interact.* 173, 1–11. doi:10.1007/s10751-007-9535-2

Burbidge, E. M., Burbidge, G. R., Fowler, W. A., and Hoyle, F. (1957). Synthesis of the elements in stars. *Rev. Mod. Phys.* 29, 547–650. doi:10.1103/RevModPhys.29.547

Busso, M., Picchio, G., Gallino, R., and Chieffi, A. (1988). Are s-elements really produced during thermal pulses in intermediate-mass stars?. *Astrophys. J.*, 196. doi:10.1086/166081

Busso, M., Gallino, R., and Wasserburg, G. J. (1999). Nucleosynthesis in asymptotic giant branch stars: Relevance for galactic enrichment and solar system formation. *Annu. Rev. Astron. Astrophys.* 37, 239–309. doi:10.1146/annurev.astro.37.1.239

Busso, M., Vescovi, D., Palmerini, S., Cristallo, S., and Antonuccio-Delogu, V. (2021). s-Processing in AGB stars revisited. III. Neutron captures from MHD mixing at different metallicities and observational constraints. *Astrophys. J.* 908, 55. doi:10.3847/1538-4357/abca8e

Busso, M., Wasserburg, G. J., Nollett, K. M., and Calandra, A. (2007). Can extra mixing in RGB and AGB stars Be attributed to magnetic mechanisms? *Astrophys. J.* 671, 802–810. doi:10.1086/522616

Cameron, A. G. W. (1957). Nuclear reactions in stars and nucleogenesis. *Publ. Astron. Soc. Pac.* 69, 201. doi:10.1086/127051

Coryell, C. D. (1956). *MITL.N.S. Prog. Rep. AECU-3423*.

Coryell, C. D. (1961). The chemistry of creation of the heavy elements. *J. Chem. Educ.* 38, 67. doi:10.1021/ed038p67

Cowan, J. J., Thielemann, F.-K., and Truran, J. W. (1991). The R-process and nucleochronology. *Phys. Rep.* 208, 267–394. doi:10.1016/0370-1573(91)90070-3

Cristallo, S., Piersanti, L., Straniero, O., Gallino, R., Domínguez, I., Abia, C., et al. (2011). Evolution, nucleosynthesis, and yields of low-mass asymptotic giant branch stars at different metallicities. II. The FRUITY database. *Astrophys. J. Suppl. Ser.* 197, 17. doi:10.1088/0067-0049/197/2/17

Cristallo, S., Straniero, O., Piersanti, L., and Gobrecht, D. (2015). Evolution, nucleosynthesis, and yields of AGB stars at different metallicities. III. Intermediate-Mass models, revised low-mass models, and the ph-FRUITY interface. *Astrophys. J. Suppl. Ser.* 219, 40. doi:10.1088/0067-0049/219/2/40

Denissenkov, P. A., Pinsonneault, M., and MacGregor, K. B. (2009). Magneto-thermohaline mixing in red giants. *Astrophys. J.* 696, 1823–1833. doi:10.1088/0004-637X/696/2/1823

Denissenkov, P. A., and Tout, C. A. (2003). Partial mixing and formation of the ^{13}C pocket by internal gravity waves in asymptotic giant branch stars. *Mon. Not. R. Astron. Soc.* 340, 722–732. doi:10.1046/j.1365-8711.2003.06284.x

Dillmann, I., Heil, M., Käppeler, F., Plag, R., Rauscher, T., and Thielemann, F. K. (2006). "KADoNiS- the Karlsruhe astrophysical database of nucleosynthesis in stars," in *Capture gamma-ray spectroscopy and related topics. Vol. 819 of American Institute of physics conference series*. Editors A. Woehr and A. Aprahamian, 123–127. doi:10.1063/1.2187846

Dillmann, I. (2014). "The new KADoNiS v1.0 and its influence on the s-process," in *XIII nuclei in the cosmos (NIC XIII)*, 57.

Evans, P. A., Cenko, S. B., Kennea, J. A., Emery, S. W. K., Kuin, N. P. M., Korobkin, O., et al. (2017). Swift and NuSTAR observations of GW170817: Detection of a blue kilonova. *Science* 358, 1565–1570. doi:10.1126/science.aap9580

Farouqi, K., Kratz, K. L., and Pfeiffer, B. (2009). Co-production of light p-s- and r-process isotopes in the high-entropy wind of type II supernovae. *Publ. Astron. Soc. Aust.* 26, 194–202. doi:10.1071/AS08075

Farouqi, K., Kratz, K. L., Pfeiffer, B., Rauscher, T., Thielemann, F. K., and Truran, J. W. (2010). Charged-particle and neutron-capture processes in the high-entropy wind of core-collapse supernovae. *Astrophys. J.* 712, 1359–1377. doi:10.1088/0004-637X/712/2/1359

Farouqi, K., Thielemann, F.-K., Rosswog, S., and Kratz, K.-L. (2022). Correlations of r-process elements in very metal-poor stars as clues to their nucleosynthesis sites. *Astron. Astrophys.* 663, A70. in press. doi:10.1051/0004-6361/202141038

Freiburghaus, C., Rembges, J. F., Rauscher, T., Kolbe, E., Thielemann, F. K., Kratz, K. L., et al. (1999a). The astrophysical r-process: A comparison of calculations following adiabatic expansion with classical calculations based on neutron densities and temperatures. *Astrophys. J.* 516, 381–398. doi:10.1086/307072

Freiburghaus, C., Rosswog, S., and Thielemann, F. K. (1999b). [CLC] [ITAL]r [/ITAL] [/CLC]-Process in neutron star mergers. *Astrophys. J.* 525, L121–L124. doi:10.1086/312343

Gallino, R., Busso, M., Picchio, G., Raiteri, C. M., and Renzini, A. (1988). On the role of low-mass asymptotic giant branch stars in producing a solar system distribution of s-process isotopes. *Astrophys. J.* 334, L45. doi:10.1086/185309

Guerrero, C., Boccone, V., Brugger, M., Calviani, M., Cerutti, F., Chiaveri, E., et al. (2013). "The latest on neutron-induced capture and fission measurements at the CERN n_TOF facility," in *Capture gamma-ray spectroscopy and related topics*. Editor P. E. Garrett, 354–364. doi:10.1142/9789814383646_0047

Herwig, F. (2005). Evolution of asymptotic giant branch stars. *Annu. Rev. Astron. Astrophys.* 43, 435–479. doi:10.1146/annurev.astro.43.072103.150600

Hill, V., Plez, B., Cayrel, R., Beers, T. C., Nordström, B., Andersen, J., et al. (2002). First stars. I. The extreme r-element rich, iron-poor halo giant CS 31082-001. Implications for the r-process site(s) and radioactive cosmochronology. *Astron. Astrophys.* 387, 560–579. doi:10.1051/0004-6361:20020434

Hillebrandt, W. (1978). The rapid neutron-capture process and the synthesis of heavy and neutron-rich elements. *Space Sci. Rev.* 21, 639–702. doi:10.1007/BF00186236

Honda, S., Aoki, W., Ishimaru, Y., and Wanajo, S. (2007). Neutron-capture elements in the very metal-poor star HD 88609: Another star with excesses of light neutron-capture elements. *Astrophys. J.* 666, 1189–1197. doi:10.1086/520034

Iben, J. I., and Renzini, A. (1982). On the formation of carbon star characteristics and the production of neutron-rich isotopes in asymptotic giant branch stars of small core mass. *Astrophys. J.* 263, L23–L27. doi:10.1086/183916

Iben, J. I., and Truran, J. W. (1978). On the surface composition of thermally pulsing stars of high luminosity and on the contribution of such stars to the element enrichment of the interstellar medium. *Astrophys. J.* 220, 980–995. doi:10.1086/155986

Ji, A. P., Drout, M. R., and Hansen, T. T. (2019). The lanthanide fraction distribution in metal-poor stars: A test of neutron star mergers as the dominant r-process site. *Astrophys. J.* 882, 40. doi:10.3847/1538-4357/ab3291

Kaeppeler, F., Gallino, R., Busso, M., Picchio, G., and Raiteri, C. M. (1990). S-process nucleosynthesis: Classical approach and asymptotic giant branch models for low-mass stars. *Astrophys. J.* 354, 630. doi:10.1086/168720

Käppeler, F., Gallino, R., Bisterzo, S., and Aoki, W. (2011). Theprocess: Nuclear physics, stellar models, and observations. *Rev. Mod. Phys.* 83, 157–193. doi:10.1103/RevModPhys.83.157

Karakas, A. I., and Lattanzio, J. C. (2014). The dawes review 2: Nucleosynthesis and stellar yields of low- and intermediate-mass single stars. *Publ. Astron. Soc. Aust.* 31, e030. doi:10.1017/pasa.2014.21

Kratz, K.-L., Akram, W., Farouqi, K., and Hallmann, O. (2019). "Production of light trans-Fe elements in core collapse-supernovae: Implications from presolar SiC-X grains," in *Exotic nuclei and nuclear/particle AstroPhysics (VII). Physics with small accelerators. Vol. 2076 of American Institute of physics conference series*, 030002. doi:10.1063/1.5091628

Kratz, K.-L., Bitouzet, J.-P., Thielemann, F.-K., Moeller, P., and Pfeiffer, B. (1993). Isotopic r-process abundances and nuclear structure far from stability: Implications for the r-process mechanism. *Astrophys. J.* 403, 216. doi:10.1086/172196

Kratz, K.-L., Farouqi, K., and Möller, P. (2014). A high-entropy-wind r-process study based on nuclear-structure quantities from the new finite-range droplet model frdm(2012). *Astrophys. J.* 792, 6. doi:10.1088/0004-637X/792/1/6

Kratz, K.-L., Farouqi, K., Pfeiffer, B., Truran, J. W., Sneden, C., and Cowan, J. J. (2007). Explorations of the r-processes: Comparisons between calculations and observations of low-metallicity stars. *Astrophys. J.* 662, 39–52. doi:10.1086/517495

Kratz, K.-L., Pfeiffer, B., Thielemann, F.-K., and Walters, W. B. (2000). Nuclear structure studies at ISOLDE and their impact on the astrophysical r-process. *Hyperfine Interact.* 129, 185–221. doi:10.1023/A:1012694723985

Kratz, K. L., Böhmer, W., Freiburghaus, C., Möller, P., Pfeiffer, B., Rauscher, T., et al. (2001). On the origin of the Ca-Ti-Cr isotopic anomalies in the inclusion EK-1-4-1 of the Allende-meteorite. *Mem. Soc. Astron. It.* 72, 453–466.

Kratz, K. L., Farouqi, K., Mashonkina, L. I., and Pfeiffer, B. (2008). Nucleosynthesis modes in the high-entropy-wind of type II supernovae. *New Astron. Rev.* 52, 390–395. doi:10.1016/j.newar.2008.06.015

Kratz, K. L., Gabelmann, H., Möller, P., Pfeiffer, B., Ravn, H. L., and Wöhr, A. (1991). Neutron-rich isotopes around the r-process "waiting-point" nuclei ${\$\mmultiscripts{\mathrm{/}}{\postscript{}{79}}{\prescript{29}{}}{}\$}Cu_{50}$ and ${\$\mmultiscripts{\mathrm{/}}{\postscript{}{80}}{\prescript{30}{}}{}\$}Zn_{50}$. *Zeitschrift fur Physik A Hadrons Nucl.* 340, 419–420. doi:10.1007/BF01290331

Kratz, K. L. (1988). Nuclear physics constraints to bring the astrophysical R-process to the "waiting point". *Rev. Mod. Astronomy* 1, 184–209. doi:10.1007/978-3-642-74188-3_9

Kratz, K. L., Ziegert, W., Hillebrandt, W., and Thielemann, F. K. (1983a). Determination of stellar neutron-capture rates for radioactive nuclei with the aid of beta-delayed neutron emission. *Astron. & Astrophys.* 125, 381–387.

Kratz, K. L., Ziegert, W., Thielemann, F. K., and Hillebrandt, W. (1983b). Beta-delayed neutron emission as the inverse process to neutron-capture on radioactive isotopes. *Max Planck Inst. fur Astrophys. Rep.* 90, 111–112.

Lattimer, J. M., Mackie, F., Ravenhall, D. G., and Schramm, D. N. (1977). The decompression of cold neutron star matter. *Astrophys. J.* 213, 225–233. doi:10.1086/155147

Lhersonneau, G., Pfeiffer, B., Kratz, K. L., Enqvist, T., Jauho, P. P., Jokinen, A., et al. (1994). Evolution of deformation in the neutron-rich Zr region from excited intruder state to the ground state. *Phys. Rev. C* 49, 1379–1390. doi:10.1103/PhysRevC.49.1379

Li, K.-A., Qi, C., Lugaro, M., Yagüe López, A., Karakas, A. I., den Hartogh, J., et al. (2021). The stellar β-decay rate of ^{134}Cs and its impact on the barium nucleosynthesis in the s-process. *Astrophys. J. Lett.* 919, L19. doi:10.3847/2041-8213/ac260f

Litvinov, Y. A., and Bosch, F. (2011). Beta decay of highly charged ions. *Rep. Prog. Phys.* 74, 016301. doi:10.1088/0034-4885/74/1/016301

Liu, N., Savina, M. R., Davis, A. M., Gallino, R., Straniero, O., Gyngard, F., et al. (2014). Barium isotopic composition of mainstream silicon carbides from murchison: Constraints for s-process nucleosynthesis in asymptotic giant branch stars. *Astrophys. J.* 786, 66. doi:10.1088/0004-637X/786/1/66

Liu, N., Savina, M. R., Gallino, R., Davis, A. M., Bisterzo, S., Gyngard, F., et al. (2015). Correlated strontium and barium isotopic compositions of acid-cleaned single mainstream silicon carbides from murchison. *Astrophys. J.* 803, 12. doi:10.1088/0004-637X/803/1/12

Lodders, K. (2021). Relative atomic solar system Abundances, mass fractions, and atomic masses of the elements and their isotopes, composition of the solar photosphere, and compositions of the major chondritic meteorite groups. *Space Sci. Rev.* 217, 44. doi:10.1007/s11214-021-00825-8

Lugaro, M., Karakas, A. I., Stancliffe, R. J., and Rijs, C. (2012). The s-process in asymptotic giant branch stars of low metallicity and the composition of carbon-enhanced metal-poor stars. *Astrophys. J.* 747, 2. doi:10.1088/0004-637X/747/1/2

Maiorca, E., Magrini, L., Busso, M., Randich, S., Palmerini, S., and Trippella, O. (2012). News on the s process from young open clusters. *Astrophys. J.* 747, 53. doi:10.1088/0004-637X/747/1/53

Mascali, D., Busso, M., Mengoni, A., Amaducci, S., Giuseppe, C., Celona, L., et al. (2020). "The PANDORA project: An experimental setup for measuring in-plasma β-decays of astrophysical interest," in *European physical journal web of conferences. Vol. 227 of European physical journal web of conferences*, 01013. doi:10.1051/epjconf/202022701013

Mashonkina, L., and Christlieb, N. (2014). The Hamburg/ESO R-process Enhanced Star survey (HERES). IX. Constraining pure r-process Ba/Eu abundance ratio from observations of r-II stars. *Astron. Astrophys.* 565, A123. doi:10.1051/0004-6361/201423651

Mashonkina, L. I., and Belyaev, A. K. (2019). Even-to-Odd barium isotope ratio in selected galactic halo stars. *Astron. Lett.* 45, 341–352. doi:10.1134/S1063773719060033

Mashonkina, L. I., Vinogradova, A. B., Ptitsyn, D. A., Khokhlova, V. S., and Chernetsova, T. A. (2007). Neutron-capture elements in halo, thick-disk, and thin-disk stars. Strontium, yttrium, zirconium, cerium. *Astron. Rep.* 51, 903–919. doi:10.1134/S1063772907110042

Merrill, P. W. (1952). Spectroscopic observations of stars of class. *Astrophys. J.* 116, 21. doi:10.1086/145589

Möller, P., Pfeiffer, B., and Kratz, K.-L. (2003). New calculations of gross β-decay properties for astrophysical applications: Speeding-up the classical r process. *Phys. Rev. C* 67, 055802. doi:10.1103/PhysRevC.67.055802

Montes, F., Beers, T. C., Cowan, J., Elliot, T., Farouqi, K., Gallino, R., et al. (2007). Nucleosynthesis in the early Galaxy. *Astrophys. J.* 671, 1685–1695. doi:10.1086/523084

Niederer, F. R., Papanastassiou, D. A., and Wasserburg, G. J. (1980). Endemic isotopic anomalies in titanium. *Astrophys. J.* 240, L73–L77. doi:10.1086/183326

Nishimura, N., Sawai, H., Takiwaki, T., Yamada, S., and Thielemann, F. K. (2017). The intermediate r-process in core-collapse supernovae driven by the magneto-rotational instability. *Astrophys. J.* 836, L21. doi:10.3847/2041-8213/aa5dee

Nordhaus, J., Busso, M., Wasserburg, G. J., Blackman, E. G., and Palmerini, S. (2008). Magnetic mixing in red giant and asymptotic giant branch stars. *Astrophys. J.* 684, L29–L32. doi:10.1086/591963

Nucci, M. C., and Busso, M. (2014). Magnetohydrodynamics and deep mixing in evolved stars. I. Two- and three-dimensional analytical models for the asymptotic giant branch. *Astrophys. J.* 787, 141. doi:10.1088/0004-637X/787/2/141

Palmerini, S., Busso, M., Vescovi, D., Naselli, E., Pidatella, A., Mucciola, R., et al. (2021). Presolar grain isotopic ratios as constraints to nuclear and stellar parameters of asymptotic giant branch star nucleosynthesis. *Astrophys. J.* 921, 7. doi:10.3847/1538-4357/ac1786

Pearson, C., Krueger, M., and Ganz, E. (1996). Direct tests of microscopic growth models using hot scanning tunneling microscopy movies. *Phys. Rev. Lett.* 76, 2306–2309. doi:10.1103/PhysRevLett.76.2306

Pellin, M. J., Savina, M. R., Calaway, W. F., Tripa, C. E., Barzyk, J. G., Davis, A. M., et al. (2006). "Heavy metal isotopic anomalies in supernovae presolar grains," in *37th annual lunar and planetary science conference. Lunar and planetary science conference*. Editors S. Mackwell and E. Stansbery, 2041.

Pfeiffer, B., Kratz, K. L., and Thielemann, F. K. (1997). Analysis of the solar-system r-process abundance pattern with the new ETFSI-Q mass formula. *Z. Phys. A -. Part. Fields.* 357, 235–238. doi:10.1007/s002180050237

Pfeiffer, B., Lhersonneau, G., Gabelmann, H., and Kratz, K. L.the ISOLDE-Collaboration (2002). *A tentative 4- isomeric state in Sr-98. arXiv e-prints* , nucl-ex/0202025.

Prantzos, N. (2019). Galactic chemical evolution with rotating massive star yields. *Nucl. Cosmos XV* 219, 83–89. doi:10.1007/978-3-030-13876-9_1

Reifarth, R., Erbacher, P., Fiebiger, S., Göbel, K., Heftrich, T., Heil, M., et al. (2018). Neutron-induced cross sections. From raw data to astrophysical rates. *Eur. Phys. J. Plus* 133, 424. doi:10.1140/epjp/i2018-12295-3

Rosswog, S., Liebendörfer, M., Thielemann, F. K., Davies, M. B., Benz, W., and Piran, T. (1999). Mass ejection in neutron star mergers. *Astron. & Astrophys.* 341, 499–526.

Rosswog, S., Sollerman, J., Feindt, U., Goobar, A., Korobkin, O., Wollaeger, R., et al. (2018). The first direct double neutron star merger detection: Implications for cosmic nucleosynthesis. *Astron. Astrophys.* 615, A132. doi:10.1051/0004-6361/201732117

Salpeter, E. E. (1955). The luminosity function and stellar evolution. *Astrophys. J.* 121, 161. doi:10.1086/145971

Seeger, P. A., Fowler, W. A., and Clayton, D. D. (1965). Nucleosynthesis of heavy elements by neutron capture. *Astrophys. J. Suppl. Ser.* 11, 121. doi:10.1086/190111

Shibata, K., Iwamoto, O., Nakagawa, T., Iwamoto, N., Ichihara, A., Kunieda, S., et al. (2011). JENDL-4.0: A new library for innovative nuclear energy systems. *J. Korean Phys. Soc.* 59, 1046–1051. doi:10.3938/jkps.59.1046

Sneden, C., Cowan, J. J., Lawler, J. E., Ivans, I. I., Burles, S., Beers, T. C., et al. (2003). The extremely metal-poor, neutron capture-rich star CS 22892-052: A comprehensive abundance analysis. *Astrophys. J.* 591, 936–953. doi:10.1086/375491

Sneden, C., McWilliam, A., Preston, G. W., Cowan, J. J., Burris, D. L., and Armosky, B. J. (1996). The ultra–metal-poor, neutron-capture–rich giant star CS 22892-052. *Astrophys. J.* 467, 819. doi:10.1086/177656

Stephan, T., and Davis, A. M. (2021). Molybdenum isotope dichotomy in meteorites caused by s-process variability. *Astrophys. J.* 909, 8. doi:10.3847/1538-4357/abd725

Stephan, T., Trappitsch, R., Davis, A. M., Pellin, M. J., Rost, D., Savina, M. R., et al. (2018). Strontium and barium isotopes in presolar silicon carbide grains measured with CHILI-two types of X grains. *Geochim. Cosmochim. Acta* 221, 109–126. doi:10.1016/j.gca.2017.05.001

Stephan, T., Trappitsch, R., Hoppe, P., Davis, A. M., Pellin, M. J., and Pardo, O. S. (2019). Molybdenum isotopes in presolar silicon carbide grains: Details of s-process nucleosynthesis in parent stars and implications for r- and p-processes. *Astrophys. J.* 877, 101. doi:10.3847/1538-4357/ab1c60

Suess, H. E., and Urey, H. C. (1956). Abundances of the elements. *Rev. Mod. Phys.* 28, 53–74. doi:10.1103/RevModPhys.28.53

Taioli, S., Vescovi, D., Busso, M., Palmerini, S., Cristallo, S., Mengoni, A., et al. (2021). Theoretical estimate of the half-life for the radioactive ^{134}Cs and ^{135}Cs in astrophysical scenarios. *arXiv e-prints, Ap.J* 2022. in press, arXiv:2109.14230.

Takahashi, K., Witti, J., and Janka, H. T. (1994). Nucleosynthesis in neutrino-driven winds from protoneutron stars II. The r-process. *Astron. & Astrophys.* 286, 857–869.

Takahashi, K., and Yokoi, K. (1987). Beta-decay rates of highly ionized heavy atoms in stellar interiors. *Atomic Data Nucl. Data Tables* 36, 375–409. doi:10.1016/0092-640X(87)90010-6

Theis, C., Käppeler, F., Wisshak, K., and Voss, F. (1998). On the puzzling origin of the rare in and SN isotopes. *Astrophys. J.* 500, 1039–1048. doi:10.1086/305777

Travaglio, C., Gallino, R., Arnone, E., Cowan, J., Jordan, F., and Sneden, C. (2004). Galactic evolution of Sr, Y, and Zr: A multiplicity of nucleosynthetic processes. *Astrophys. J.* 601, 864–884. doi:10.1086/380507

Trippella, O., Busso, M., Palmerini, S., Maiorca, E., and Nucci, M. C. (2016). s-Processing in AGB stars revisited. II. Enhanced 13C production through MHD-induced mixing. *Astrophys. J.* 818, 125. doi:10.3847/0004-637X/818/2/125

Vescovi, D., Cristallo, S., Busso, M., and Liu, N. (2020). Magnetic-buoyancy-induced mixing in AGB stars: Presolar SiC grains. *Astrophys. J.* 897, L25. doi:10.3847/2041-8213/ab9fa1

Vescovi, D., Cristallo, S., Palmerini, S., Abia, C., and Busso, M. (2021). Magnetic-buoyancy-induced mixing in AGB stars: Fluorine nucleosynthesis at different metallicities. *Astron. Astrophys.* 652, A100. doi:10.1051/0004-6361/202141173

Vescovi, D. (2021). Mixing and magnetic fields in asymptotic giant branch stars in the framework of FRUITY models. *Universe* 8, 16. doi:10.3390/universe8010016

Vescovi, D., and Reifarth, R. (2021). s-Processing in asymptotic giant branch stars in the light of revised neutron-capture cross sections. *Universe* 7, 239. doi:10.3390/universe7070239

Wasserburg, G. J., Lee, T., and Papanastassiou, D. A. (1977). Correlated O And Mg isotopic anomalies in Allende Inclusions: II. Magnesium. *Geophys. Res. Lett.* 4, 299–302. doi:10.1029/GL004i007p00299

Wisshak, K., Voss, F., Käppeler, F., Kazakov, L., Bečvář, F., Krtička, M., et al. (2006b). Fast neutron capture on the Hf isotopes: Cross sections, isomer production, and stellar aspects. *Phys. Rev. C* 73, 045807. doi:10.1103/PhysRevC.73.045807

Wisshak, K., Voss, F., Käppeler, F., and Kazakov, L. (2006a). Stellar neutron capture cross sections of the Lu isotopes. *Phys. Rev. C* 73, 015807. doi:10.1103/PhysRevC.73.015807

Woosley, S. E., Wilson, J. R., Mathews, G. J., Hoffman, R. D., and Meyer, B. S. (1994). The r-process and neutrino-heated supernova ejecta. *Astrophys. J.* 433, 229. doi:10.1086/174638

Appendix 1: Some comments on stellar models

A general, synthetic outline of the stellar parents of neutron-rich elements beyond iron can be found in El Eid (2018). We briefly comment on these astrophysical sources below, believing that this brief summary can be sufficient for an article, which is mainly devoted to nuclear, not stellar, effects.

Stellar models for the *s*-process

Beyond the *main s*-process component discussed in this study, it is well-known that another, less effective, slow neutron capture process exists, where massive stars ($M \geq 10\,M_\odot$) contribute to the production of heavy elements between $A = 60$ and $A = 90$, in what is called the *weak s*-process (occurring during core-He and shell-C burning phases, mainly thanks to the activation of the $^{22}\mathrm{Ne}(\alpha,\mathrm{n})^{25}\mathrm{Mg}$ reaction). Rotation can also boost this *s*-process component in massive star models of low metallicity, letting it reach higher atomic masses. While we do not address these issues here, interested readers can find details in Pignatari et al. (2010) and Nishimura et al. (2017).

Rather, some words must be spent on the mixing mechanisms driving the formation of the neutron source $^{13}\mathrm{C}(\alpha,\mathrm{n})^{16}\mathrm{O}$ in AGB stars, generating the main component discussed in the previous sections. The general characteristics that these mixing phenomena must have were outlined a few years ago in Busso et al. (2011) and further specified in Nucci and Busso (2014). In the first of these contributions, it was shown that the most common extra-mixing mechanisms explored in stellar evolution (like thermohaline diffusion and various types of rotationally-induced mass transport) would be too slow and ineffective to produce adequate circulation at the H–He interface. It was also argued that a faster process, like magnetic buoyancy, might instead provide the required effects.

While this last mechanism was, indeed, explored by us in recent years and used also in the present study, other physical processes might obtain the same effects. In particular, in Nucci and Busso (2014) it was shown that the geometrical simplifications adopted in our MHD model are equivalent to establish buoyancy with a velocity growing at least quadratically with radius. Any mechanism performing this might then be used, as well. Among promising physical phenomena certainly occurring in stars, but not explored sufficiently so far, we can mention gravity waves (Battino et al., 2016, 2019), and in general

any wave-like propagation including some transport of mass. We believe looking for such possible alternatives to MHD mixing would be very important and probably highly rewarding. The first thing to be verified would be the ability of such transport mechanisms to provide the extended pockets with *flat* $^{13}\mathrm{C}$ distributions, which were shown to be necessary by Liu et al. (2015). They would also imply the same reduction in $^{14}\mathrm{N}$ and the same low values of the neutron density discussed in the present article.

Stellar models for the *r*-process

Rather recently (2017), the *White paper on Nuclear Astrophysics* recognized (Arcones et al., 2017), among the main open problems in our understanding of the origin of the elements, some crucial issues concerning the fast neutron captures. Among other things, there were questions like 1) "where are the 54 elements beyond iron created that are traditionally attributed to a rapid neutron capture process (*r*-process)?" and 2) "what is the contribution of neutrino-driven winds in core collapse supernovae (ccSNe) to nucleosynthesis and what role do neutrino properties play?" Despite the fact that, in the same year, observations from the kilonova associated to the gravitational wave source GW170817 became available, the same questions remain unanswered now. Indeed, while it seems clear that in the kilonova ejecta there were regions whose high opacities are in line with lanthanide-rich materials (Stratta, 2019) and while also lines of Sr and Y have been observed (Vieira 586 et al., 2022), it appears that the kilonova did not produce a typical solar-like *r*-process distribution (Ji et al., 2019). Other sources, like collapsars (Siegel et al., 2019) and *ccSNe* (Suzuki et al., 2019) remain on the stage, in this last case with results remarkably dependent on the nuclear mass model adopted for determining β decays for waiting-point nuclei.

In the present, still uncertain, situation, we remind what has been said in Section 3, commenting Figure 3. The heavier nuclei of the third panel in the figure are today commonly attributed to *NSM* of various types, while the lighter isotopes of panel 1 can still be safely ascribed to *ccSNe* (Yamazaki et al., 2022). For the intermediate distribution of panel 2 (corresponding to a *weak* or *incomplete r*-process) best candidates remain jet-like magneto-rotational supernovae (Nishimura et al., 2017; Farouqi et al., 2022). Contributions might come also from jet-like emissions in *NSM* (Yamazaki et al., 2022) and from collapsars (Siegel et al., 2019).